particles

Tracked for Impact Factor

Indexed in: Scopus

Article

Probing the Hot QCD Matter via Quarkonia at the Next-Generation Heavy-Ion Experiment at LHC

Yuri Kharlov, Yeghishe Hambardzumyan and Antony Varlamov

MDPI

https://doi.org/10.3390/particles6020030

particles

Article

Probing the Hot QCD Matter via Quarkonia at the Next-Generation Heavy-Ion Experiment at LHC

Yuri Kharlov [1,2,*,†], Yeghishe Hambardzumyan [2,†] and Antony Varlamov [2,†]

[1] NRC "Kurchatov Institute"—IHEP, Protvino 142281, Russia
[2] Moscow Institute of Physics and Technology, Dolgoprodny 141701, Russia; yeghishe.hambardzumyan@cern.ch (Y.H.); varlamov.am@phystech.edu (A.V.)
* Correspondence: yuri.kharlov@cern.ch
† These authors contributed equally to this work.

Abstract: Quarkonia represent one of the most valuable probes of the deconfined quark–gluon hot medium since the very first experimental studies with ultrarelativistic heavy-ion collisions. A significant step forward in characterizing the QCD matter via systematic studies of quarkonia production will be performed by the next-generation heavy-ion experiment ALICE 3, a successor of the ongoing ALICE experiment at the Large Hadron Collider. The new advanced detector of ALICE 3 will allow for exploring the production of S- and P-state quarkonia at high statistics, at low and moderate transverse momenta ranges. The performance of ALICE 3 for quarkonia measurements and the requirements for the detectors are discussed.

Keywords: ultrarelativistic proton and heavy-ion collisions; LHC; heavy quarks; quarkonium; detector performance; simulations

Citation: Kharlov, Y.; Hambardzumyan, Y.; Varlamov, A. Probing the Hot QCD Matter via Quarkonia at the Next-Generation Heavy-Ion Experiment at LHC. *Particles* **2023**, *6*, 546–555. https://doi.org/10.3390/particles6020030

Academic Editor: Peter Senger

Received: 1 February 2023
Revised: 16 April 2023
Accepted: 28 April 2023
Published: 2 May 2023

1. Introduction

Quantum chromodynamics predicts the existence of a new state of matter, in which the quarks and gluons are deconfined, that is, not bound into colorless hadrons. Experimental studies on this state of strongly interacting matter consider several key probes, such as electromagnetic signals in the form of the emission of real or virtual photons, jets carrying information about the leading partons, heavy-flavor mesons, quarkonia, and various bulk effects. The theory of strong interactions tries to describe the behaviors of these probes in the medium at finite temperature. Among the above-mentioned probes, quarkonia production is a candle probe, having thoroughly been studied over the last three decades.

Studying the yields of quarkonia and of the bound states of heavy quark and antiquark in ultrarelativistic heavy-ion collisions is one of the key experimental probe for the properties of the quark–gluon deconfined medium. Heavy quarks are produced at the beginning of the collision, and therefore, they experience the entire evolution of the quark–gluon medium produced in heavy-ion collisions. Various mechanisms affect the production of bound states $c\bar{c}$ and $b\bar{b}$ [1–3]:

- The binding of heavy quarks is suppressed due to color screening;
- Once the bound state is formed, it may dissociate in the process of interaction with the medium;
- If there are enough $Q\bar{Q}$ pairs, quarkonium states can be formed, either at the freeze-out or inside the quark–gluon medium, in a process that is referred to as recombination [3,4].

The pair of heavy quark and antiquark $Q\bar{Q}$ can create a bound state at a binding radius r_i. The color screening radius $r_D(T)$ in the deconfined medium of color charges decreases with temperature T, which leads to a stronger color screening of heavy quarks Q. If $r_D(T)$ is smaller than r_i, the quarkonium state cannot exist. The quarkonium dissociation temperature T_i defined by $r_D(T) \approx r_i$, and this determines the thermodynamic properties

of the medium, and energy density and temperature, at which the quarkonium yield is modified compared to the yield in vacuum [1], and obviously, different quarkonia states behave differently because of their different binding radii and binding energies.

From these considerations, one can conclude that the production measurements of quarkonium states with different binding radii r_i and different binding energies E_i would serve as a sensitive probe of the quark–gluon medium thermodynamic properties. From an experimental point of view, the most attractive charmonia are those with masses that are less than the double masses of D-mesons. The properties of charmonia of interest are presented tn the Table 1.

Table 1. Properties of charmonium states of interest for studying quark–gluon matter.

Particle	Mass (MeV/c^2)	Binding Energy (MeV)	Decay Channel	Branching (%)
J/ψ (1S)	3096.90	0.64	$J/\psi \to e^+e^-, \mu^+\mu^-$	5.971
χ_{c0} (1P)	3414.75	0.32	$\chi_{c0} \to J/\psi\gamma$	1.27
χ_{c1} (1P)	3510.66	0.22	$\chi_{c1} \to J/\psi\gamma$	33.9
χ_{c2} (1P)	3556.20	0.18	$\chi_{c2} \to J/\psi\gamma$	19.2

Systematic simultaneous measurements of different charmonia states with the same experiment are necessary to disentangle the various mechanisms responsible for quarkonium production and its further evolution in the QCD matter. Measurements of (1P) states, $\chi_{cJ}, J = 0, 1, 2$ are also needed for the precise discrimination of prompt and non-prompt J/ψ, since χ_{cJ} is a dominant source of feed-down J/ψ.

One of the first evidence of the existence of deconfined quark–gluon matter was the observation of J/ψ suppression in Pb–Pb collisions at $\sqrt{s_{\rm NN}} = 17$ TeV, reported in the NA50 experiment at SPS [5]. The experiment observed the evolution of the J/ψ yield suppression with respect to the expected yield as a function of energy density ε. The first drop of the J/ψ yield at $\varepsilon > 2.3$ GeV/fm^3 was attributed to the disappearance of charmonium states χ_c, which decay to J/ψ. With an increase in energy density, the more tightly bound state J/ψ becomes dissolved, which was reflected in the second kink of the J/ψ suppression at $\varepsilon > 3.1$ GeV/fm^3. The NA50 drew a conclusion that the observed suppression can be naturally anticipated and understood in a deconfinement scenario as resulting from the melting of the charmonia states above a certain energy density.

The J/ψ suppression observed at SPS was followed by extensive studies at RHIC, which measured the J/ψ production in Au–Au collisions at energies up to $\sqrt{s_{\rm NN}} = 200$ GeV (see e.g., [6]). The PHENIX experiment reported on a stronger J/ψ suppression at forward rapidity than at mid-rapidity. A variety of charmonium measurements performed at RHIC suggested a more sophisticated picture of charmonium production in hot QCD matter. The suppression description calls for variety of physics mechanisms, including gluon saturation, gluon shadowing, initial-state parton energy loss, cold nuclear matter breakup, color screening, and charm recombination.

With the start of LHC experiments in 2010, charmonium properties in quark–gluon matter were addressed with unprecedented accuracy. Similar to RHIC measurements, the ALICE experiment observed a clear J/ψ suppression in Pb–Pb collisions at $\sqrt{s_{\rm NN}} =$ 2.76 TeV at forward rapidity [7]. The suppression for central events at LHC was found to be smaller than at RHIC, despite a collision energy of more than 10 times higher, which was the first clear sign of charmonium regeneration.

A preliminary measurement of ψ (2S) suppression in Pb–Pb collisions at $\sqrt{s_{\rm NN}} = 5.02$ TeV [8] shows that ψ (2S) is almost twice as suppressed with respect to J/ψ, and that the ψ (2S) suppression does not depend on collision centrality within uncertainties, which also indicates a regeneration mechanism to be more important at a higher energy of the colliding ions.

Over the last 30 years of charmonium studies in heavy-ion collisions, experimental advances were going along with theory development. For understanding the underlying

physics of quarkonium production and its evolution in QCD medium, further precision measurements of different charmonium and bottomonium states are needed:

- Statistics enhancement via increased luminosity and faster detector readout;
- Systematic uncertainties improvement via better particle identification and background suppression;
- Direct measurements of states other than J/ψ are needed to probe the effects of color screening, dissociation, and recombination.

The next-generation heavy-ion experiment ALICE 3 at LHC will pursue these studies in Run 5 and beyond.

2. The Experiment at ALICE 3

A concept of the next-generation experiment to explore strongly interacting matter in ion collisions at the LHC is presented in the letter of intent in [9]. The experiment will be a successor of the current ALICE experiment and will address multiple advanced measurements such as high-precision beauty measurements, open charm correlations, multicharm baryons production, electromagnetic radiation, chiral symmetry restoration, systematic quarkonia studies, and many other measurements for which the potential of the ongoing experiments is limited. The running scenario of ALICE 3 aims to collect Pb–Pb data at an integrated luminosity of $\mathcal{L}_{\text{int}} = 35\ \text{nb}^{-1}$, and pp data at $\mathcal{L}_{\text{int}} = 3\ \text{fb}^{-1}$ per year.

The new experiment, as shown in Figure 1, will consist of a thin silicon vertex and tracking detector, time-of-flight (TOF) and ring imaging Cherenkov (RICH) detectors for particle identification, a forward conversion tracker (FCT) for e^+e^- reconstruction from photon conversion, an electromagnetic calorimeter (ECAL), and a muon identification detector. The setup will be embedded into the superconducting solenoidal magnet with a field of 2 T.

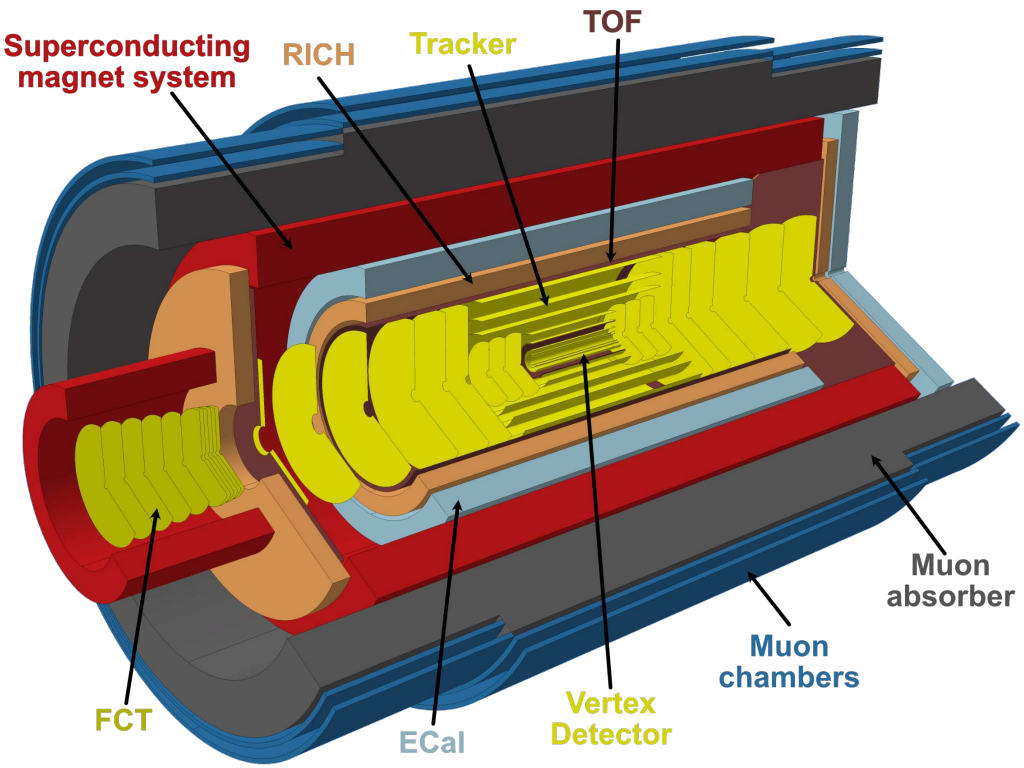

Figure 1. Conceptual layout of the ALICE 3 setup.

For charmonium measurements, the key detectors of ALICE 3 are the vertex detector with the tracker for the reconstruction of $e^{\pm}$ or $\mu^{\pm}$ tracks from J/ψ decays, ECAL for photon reconstruction from χ_c and for $e^{\pm}$ identification, and the muon detector for $\mu^{\pm}$

identification. The vertex detector and the outer tracker are based on 11 barrel layers and 2×12 discs covering the pseudorapidity interval of $|\eta| < 4$, with a longitudinal extension of $|z| < 400$ cm and a radial position from 0.5 to 80 cm. The intrinsic spatial resolutions of the tracker layers vary from 2.5 to 10 μm, and the net thickness of all layers is 9.3% of the radiation length. The outer layer of the barrel tracker, being installed at a radius of 80 cm, determines the lever arm for the track curvature measurement. The expected momentum resolution σ_p/p for muons of momentum at the multiple scattering limit $p_T = 1$ GeV/c, is between 0.6 and 1% in the pseudorapidity range $|\eta| < 2$. The CMOS Monolithic Active Pixel Sensors (MAPS) are considered as a baseline technology for the vertex detector and the outer tracker.

The electromagnetic calorimeter ECAL is designed to detect photons of low and moderate energy in a range from tens of MeV up to 50–100 GeV. In an application for charmonium measurement, the ECAL will be used for photon reconstruction from decays $\chi_{cJ} \to J/\psi\gamma$, and for $e^{\pm}$ identification. The current conceptual design of ECAL assumes that it will consist of the barrel calorimeter, with the inner bore radius $R_{\text{in}} = 115$ cm covering a pseudorapidity range of $|\eta| < 1.5$, and the end-cap calorimeters at $1.5 < \eta < 4$. The most central sector of the barrel at $|\eta| < 0.33$ will be built of the lead tungstate crystals $PbWO_4$ with high energy resolution and transverse granularity, which will be complemented by the sampling-type calorimeter at $0.33 < |\eta| < 1.5$ with a moderate resolution. Specifications of the ALICE 3 ECAL are summarized in Table 2.

Table 2. ALICE 3 ECAL specifications.

ECAL Module	Barrel Sampling	End-Cap Sampling	Barrel High-Precision
acceptance	$\Delta\varphi = 2\pi$, $\lvert\eta\rvert < 1.5$	$\Delta\varphi = 2\pi$, $1.5 < \eta < 4$	$\Delta\varphi = 2\pi$, $\lvert\eta\rvert < 0.33$
geometry	$R_{\text{in}} = 1.15$ m, $\lvert z\rvert < 2.7$ m	$0.16 < R < 1.8$ m, $z = 4.35$ m	$R_{\text{in}} = 1.15$ m, $\lvert z\rvert < 0.64$ m
technology	sampling Pb + scint.	sampling Pb + scint.	$PbWO_4$ crystals
cell size	30×30 mm^2	40×40 mm^2	22×22 mm^2
no. of channels	30,000	6000	20,000
energy range	$0.1 < E < 100$ GeV	$0.1 < E < 250$ GeV	$0.01 < E < 100$ GeV

The energy resolution is parametrized as a function of the photon energy E in GeV units via equation

$$\frac{\sigma_E}{E} = \sqrt{\left(\frac{a}{E}\right)^2 + \frac{b^2}{E} + c^2}. \quad (1)$$

The stochastic term $b/\sqrt{E}$, related to the photostatistics, is driven by the choice of the ECAL technology and the photodetector. The target value of this stochastic term is $b \approx 0.02$ GeV$^{1/2}$ for the most central barrel sector of $PbWO_4$ and $b \approx 0.11$ GeV$^{1/2}$ for the sampling-type sector. These anticipated values of the parameter b appear feasible, taking into account the current energy resolution of the ALICE PHOS and EMCal calorimeters, $b \approx 0.033$ GeV$^{1/2}$ and $b \approx 0.11$ GeV$^{1/2}$, respectively [10].

The noise term of the energy resolution a is defined by the intrinsic noises of the photodetectors, and the noise of the front-end electronics, as well as the induced noises of long signal cables. The ALICE PHOS calorimeter is characterized by $a = 13$ MeV [11], which can be improved down to a = 2–5 MeV thorough electronics design and via the use of advanced low-noise photodetectors.

A mass resolution of π^0 decay to $\gamma\gamma$ in pp collisions can serve as a candle for electromagnetic calorimeter performance. The mass resolution is obtained from the invariant mass spectra of photon pairs detected in the calorimeter, fitted to a sum of the Gaus-

sian function describing the π^0 peak, and a smooth combinatorial background. The π^0 peak parameters and the shape of the background from non-correlated photon pairs depends on the shape of the differential π^0 yield and the overall event topology. As was shown in [12], Pythia 8 with Monash 2013, [13] tune reproduces the π^0 production differential cross-section in pp collisions at $\sqrt{s} = 8$ TeV. Simulations of π^0 produced in pp collisions at $\sqrt{s} = 14$ TeV and detected in the ALICE 3 ECAL using the event generator Pythia 8.304 [14] and the parametrized ECAL response were performed to evaluate the π^0 mass resolution in the high-precision sector of ECAL built from the $PbWO_4$ crystals, as well as in the sampling calorimeter. For these studies, the Pythia process selection was set to ‘‘`SoftQCD:all = on`’’ for inelastic interactions. In addition to the ECAL response parametrization, the energy cut on photons detected in ECAL was set to $E_\gamma > 0.1$ GeV. The dependence of the mass resolution on the π^0 transverse momentum, shown in Figure 2, is consistent with the existing calorimeters PHOS and EMCal of the ALICE experiment [15]. One has to note that at high p_T, the opening angle between photons from π^0 decays becomes more narrow, so that the electromagnetic shower developed by the photons overlaps. The typical unfolding procedure of the overlapped showers is able to split such photons, as long as the distance between the photons on the front surface of a calorimeter is less than one cell. Taking into account the minimal cell size of the ALICE 3 ECAL (Table 2) and the radial distance of the ECAL from the interaction point of 115 cm, the upper limit of the π^0 transverse momentum at which the decay photons can be split is $p_T < 13$ GeV/c.

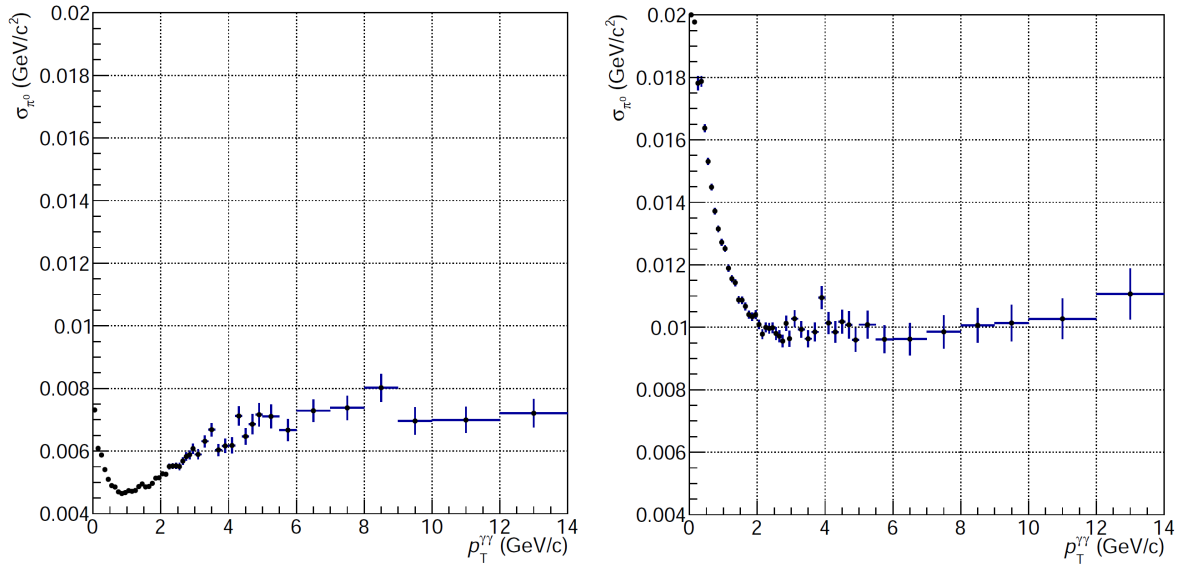

Figure 2. Mass resolution for π^0 reconstructed in the high-precision sector of ALICE 3 ECAL (**left**) and in the sector of sampling type with moderate energy resolution (**right**).

3. Performance Studies of Charmonium Measurements in ALICE 3

3.1. Event Generator

The objectives of the charmonium studies in the current work are focused on the requirements for the ALICE 3 detector performance on signal detection, and the separation of different charmonia states in proton–proton collisions at the LHC energies. These tasks rely on event generators, which reproduce the kinematic spectra of generated charmonia and their decays, as well as the relative yields of the 1P charmonium states. To select the event generator, the measured spectra of χ_{c1}, χ_{c2} production in pp collisions at the LHC energies were used. The differential cross-sections for $d\sigma/dp_T$ in pp collisions at $\sqrt{s} = 7$ TeV were measured by ATLAS [16] at mid-rapidity in the p_T range from 10 to 30 GeV/c.

The prediction of the event generator Pythia 8.304 [14] for charmonium production was compared with the ATLAS data. The configuration ‘‘`Charmonium:all = on`’’ was

set for the Pythia process selection to generate a signal event with all charmonia states; the collision system was set to pp at $\sqrt{s} = 7$ TeV. Differential cross-sections $d\sigma/dp_{\mathrm{T}}$ at $|y| < 0.5$ of χ_{c1}, χ_{c2} production calculated with Pythia are shown in Figure 3 as solid red and blue circles, whereas the ATLAS data at $10 < p_{\mathrm{T}} < 30$ GeV/c are represented by open circles. The absolute cross-sections of χ_{c1} and χ_{c2} are overestimated by Pythia at the highest p_{T} measured by ATLAS; however, the relative yields of the χ_c states are in fairly good agreement with the data, which is acceptable for the purpose of the ALICE 3 performance studies. As long as the background is not considered in the presented work, it was concluded that Pythia 8.304 is sufficient for the χ_c performance studies.

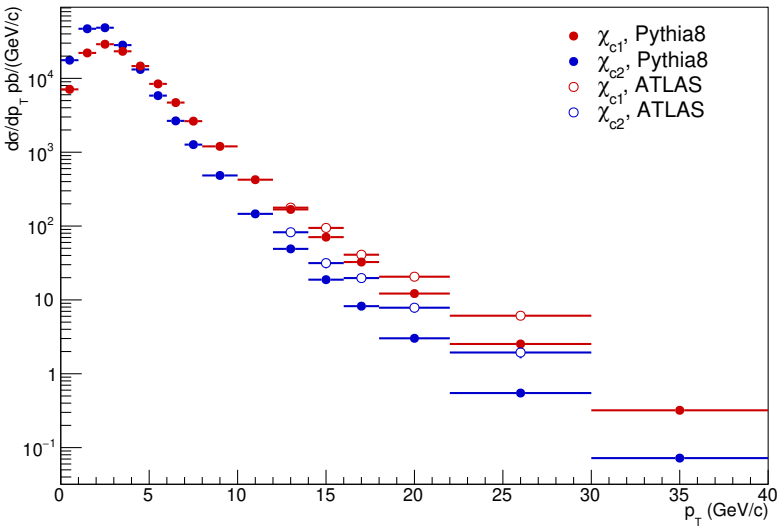

Figure 3. Comparison of production cross-sections of χ_{c1} and χ_{c2} at $|y| < 0.5$ in pp collisions at $\sqrt{s} = 7$ TeV predicted by Pythia 8.304 [14] and measured by ATLAS [16].

The feasibility of charmonium family measurements in pp collisions in the ALICE 3 detectors was studied in Monte Carlo simulations using the event generator Pythia 8.304 [14], configured for charmonium production (process selection ‘‘`Charmonium:all = on`’’) on pp collisions at energy $\sqrt{s} = 14$ TeV. In this paper, we focus on the production of the 1S state J/ψ and the 1P states χ_{c0}, χ_{c1}, and χ_{c2}, detected via decays $J/\psi \to e^+e^-$ and $\chi_{cJ} \to J/\psi\gamma$.

3.2. Event Selection and Detector Response

The detection of final-state particles from charmonia decays in ALICE 3 was evaluated in parametrized fast simulations. Electrons and positrons from J/ψ decay were selected if they had transverse momentum $p_{\mathrm{T}}^{e^\pm} > 0.1$ GeV/c, and hit the central tracker acceptance covering pseudorapidities $|\eta| < 2$ and the whole azymuthal angle $\Delta\varphi_{e^\pm} = 2\pi$. Photons from χ_{cJ} decays were detected with energies $E_\gamma > 0.1$ GeV in the most central barrel calorimeter at $|\eta_\gamma| < 0.33$ and $\Delta\varphi_\gamma = 2\pi$. The tracker barrel response function smeared the track momentum via a normal distribution with a mean value equal to the exact momentum and a standard deviation of $\sigma_p = 1\%$. The calorimeter response was parametrized by the energy resolution defined in Equation (1) with $a = 2$ MeV and $b = 0.02$ or 0.11 GeV$^{1/2}$, which correspond to a precise calorimeter from $PbWO_4$ crystals or the sampling technology, respectively.

Due to a small mass difference between χ_{cJ} and J/ψ, photons from $\chi_{cJ} \to J/\psi$ decays are rather soft. In the rest frame of χ_{cJ}, decay photons have energies of 317−459 MeV for different charmonium states. A boost of χ_{cJ} produced in collisions spreads the photon energy distribution, but the energies remain low. As for electrons and positrons from charmonium decays, their energies are determined via the mass of J/ψ, and hence, the energies are relatively high. The left panel of Figure 4 illustrates the photon energy distributions in ECAL for all three states of χ_{cJ}, $J = 0, 1, 2$. The right panel presents the energies of electrons

and positions in ECAL from χ_{cJ} decays. The dominant fraction of photons, at more than 75%, has an energy of less than 0.5 GeV where the energy resolution rises; therefore, the choice of the calorimeter technology for such low-energy photon reconstructions is crucial. Electrons, to the contrary, have energies of more than 1 GeV in 75% of cases where the ECAL resolution is satisfactory.

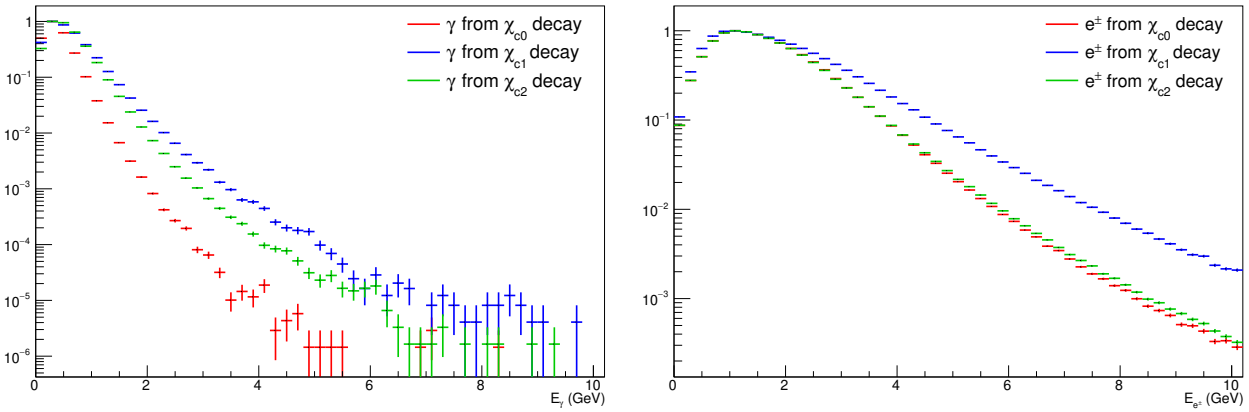

Figure 4. Photon (**left**) and electron (**right**) energy spectra in ALICE 3 ECAL from χ_{cJ} decays, $J = 0, 1, 2$.

3.3. Electron Identification

The reconstruction of J/ψ requires the momentum measurement of $e^{\pm}$ tracks in the barrel tracker and electron identification. For a high momentum of $e^{\pm}$, the energy E deposited in the ECAL is equal to the momentum p measured by the tracking system, which is $E/p = 1$. Due to the finite resolution of both the calorimeter and the tracker, the E/p is smeared, and the bremsstrahlung of electrons in the detector medium shifts the mean value of E/p from 1 to smaller values. The ability for electron identification is demonstrated by Figure 5, which shows the E/p ratio distribution in pp collisions in a similar setup of the ALICE experiment using the PHOS and the central tracking system. These two plots show a good agreement between the data (left) and the Monte Carlo simulations (right). The material budget in front of the ALICE PHOS is about 0.2 X_0, which explains a shift of the mean value of the E/p peak by -0.02 from unity. A left wing of the E/p distribution represents a background from the accidental matching of charged hadronic tracks in the central tracker, with showers in the calorimeter. The calorimeter medium discussed in Table 2 is relatively transparent for hadrons; its material budget in terms of nuclear interaction length is about $(0.7 - 1)\,\lambda_I$. Therefore, hadrons, unlike photons and electrons, deposit only a small fraction of their energy in the ECAL, and in most cases, they deposit only a minimal ionization energy loss. The experience of the ALICE experiments ensures that electron identification will have a similar performance in the future ALICE 3 experiment [15].

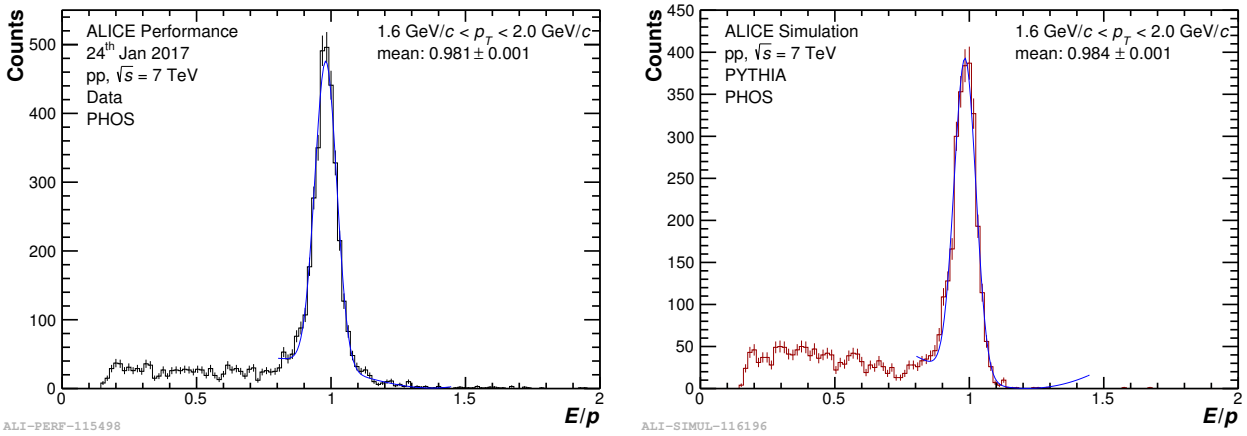

Figure 5. Ratio of energy deposited in the ALICE PHOS calorimeter to momentum, as measured by the central tracking system. (**Left**) plot are data, (**right**) plot are Monte Carlo simulations.

3.4. Charmonium Reconstruction

The first step of χ_{cJ} reconstruction requires the selection of J/ψ candidates from unlike-sign-charged tracks identified as electrons and positrons with invariant masses consistent with that of J/ψ. To quantify the J/ψ selection criteria, the invariant mass spectrum of the e^+e^- pair is fitted to the sum of the Gaussian function for the J/ψ peak, and a polynomial of the first or the second order for the background. The Gaussian part of the fit is described by the mean mass $M^0_{J/\psi}$ and the width $\sigma_{J/\psi}$. The e^+e^- pair is selected as a candidate to J/ψ if the invariant mass e^+e^- deviates from M^0_{ee} by less than $2\,\sigma_{J/\psi}$:

$$\left| M_{e^+e^-} - M^0_{J/\psi} \right| < 2\,\sigma_{J/\psi}. \tag{2}$$

The 4-momentum of the selected J/ψ candidate is calculated as a sum of the 4-momenta of the electron and positron:

$$p_{J/\psi} = p_{e^+} + p_{e^-}. \tag{3}$$

Then, the found J/ψ candidates are combined with photons detected in ECAL, and the invariant mass of J/ψ and photon pairs ($M_{\gamma J/\psi}$) is calculated. In the real experimental data, this reconstruction algorithm leads to a large number of combinations of J/ψ candidates and photons, which most probably come from different uncorrelated sources, thus generating a combinatorial background. For the purpose of the signal splitting feasibility of χ_c states, the combinations were limited only to those J/ψ and photon pairs which are the decay products of the same χ_c.

The spread of the invariant mass is affected by the momentum resolution of the $e^\pm$ tracks and the energy resolution of the photons. The tracker resolution is largely canceled in the difference of the invariant masses $\Delta M = M_{\gamma J/\psi} - M_{J/\psi}$. The spectrum of ΔM reconstructed in ALICE 3 in pp collisions at $\sqrt{s} = 14$ TeV at transverse momentum ranges over $5 < p_{\mathrm{T}} < 10$ GeV/c when photons are reconstructed in the precision sector of ECAL made of $PbWO_4$ crystals with $b = 0.02$ GeV$^{1/2}$ is shown the left plot of Figure 6. Peaks of χ_{c1} and χ_{c2} are clearly visible at $\Delta M = 0.414$ and 0.459 GeV/c^2, respectively. The peak of χ_{c0} is rather small because of a small branching ratio of decay $\chi_{c0} \to J/\psi\gamma$. For comparison, the ΔM spectrum under the assumption of the sampling calorimeter with $b = 0.11$ GeV$^{1/2}$ installed in the most central sector of ECAL is shown in the right panel of Figure 6. On both plots, the mass difference spectra are fitted to a sum of three Gaussian functions to describe individual χ_{cJ} ($J = 0, 1, 2$) peaks. In the case of the sampling calorimeter, all χ_{cJ} peaks overlap and can hardly be resolved.

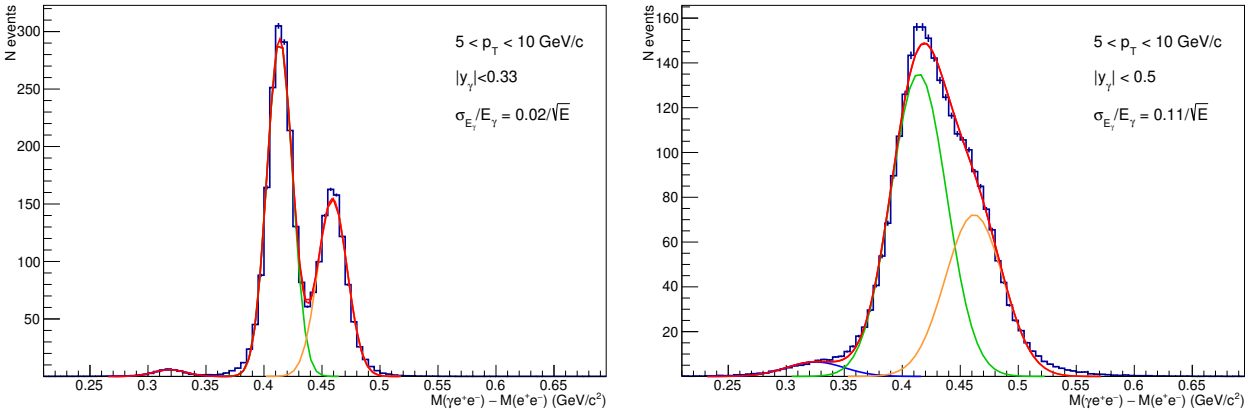

Figure 6. Invariant mass differences of $\Delta M = M_{\gamma J/\psi} - M_{J/\psi}$ for charmonium 1P states χ_{cJ}, $J = 0, 1, 2$ detected in pp collisions, with ALICE 3 assuming a precise calorimeter sector (**left**) and a calorimeter with moderate energy resolution (**right**). Spectra of ΔM are fitted to a sum of 3 Gaussian functions represented by red curves; each Gaussian contribution is represented by blue, green, and orange curves.

From these studies, we conclude that the mass resolutions of χ_{c1} and χ_{c2} are defined by the calorimeter energy resolution. Similar Monte Carlo simulations with different momentum resolution parametrizations of the central tracker σ_p/p show that the peak splitting of the ΔM spectra is independent from the momentum resolution of $e^{\pm}$ tracks.

4. Discussion

The feasibility studies of charmonium properties in the hot deconfined state of matter at the next-generation heavy-ion experiment ALICE 3 show that the main prerequisite for the measurement of J/ψ, χ_{c1} and χ_{c2} is an electromagnetic calorimeter with excellent energy resolution. A calorimeter built from the $PbWO_4$ crystals with improved light collection efficiency with respect to the ALICE PHOS detector can achieve the stochastic term of the energy resolution parametrization $b = 0.02$ GeV$^{1/2}$. A calorimeter sector with such performance, being installed in the ALICE 3 ECAL, is applicable for systematic studies of the 1S and 1P charmonium states. Further studies will pursue background evaluation and the statistical significance of the charmonium measurements at ALICE 3 under the conditions of the planned running scenario with pp and Pb–Pb collisions.

5. Conclusions

In this paper, we presented the overview of charmonium production studies in heavy-ion collisions from SPS to LHC energies. It was shown that several possible physics processes are responsible for charmonium spectrum modifications, from proton–proton to heavy-ion collisions, such as the color screening of heavy quarks, medium-induced quarkonium dissociation, and recombination. However, the accuracies of available measurements are still not sufficient to disentangle various theoretical models, which calls for new and advanced measurements at high statistics, improved systematic uncertainties, and excellent detector resolution. Such measurements should pursue the simultaneous measurements of different quarkonium states in the same experiment; especially, J/ψ (1S), ψ (2S), χ_{c1}, χ_{c2} (1P) are the most interesting probes because they have different quarkonium radii and binding energies, and these states are relatively easy to detect via their dileptonic and photonic decays.

The first feasibility studies of charmonium measurement in the future ALICE 3 experiment at LHC define the requirements for the detector specification; in particular, it is shown that χ_{c1}, χ_{c2} measurements can be performed in the experiment with the advanced electromagnetic calorimeter with excellent energy resolution, characterized by the stochastic term $b \approx 0.02$ GeV$^{1/2}$.

Data collection for the experiment at ALICE 3 is planned to start in the LHC Run 5 from 2035. Performance studies of charmonium measurements in Monte Carlo simulations will be followed by R&D studies of the detector performances of ECAL prototypes.

Author Contributions: Conceptualization, funding acquisition and supervision, Y.K.; software, data curation, formal analysis, Y.H. and A.V. All authors have read and agreed to the published version of the manuscript.

Funding: This research was funded by the RSF grant 22-42-04405.

Data Availability Statement: Data sharing is not applicable to this article.

Conflicts of Interest: The authors declare no conflict of interest.

References

1. Kluberg, L.; Satz, H. Color Deconfinement and Charmonium Production in Nuclear Collisions: *Datasheet from Landolt-Börnstein—Group I Elementary Particles, Nuclei and Atoms*; Volume 23: "Relativistic Heavy Ion Physics" in Springer Materials; Springer: Berlin/Heidelberg, Germany, 2010. [CrossRef]
2. Matsui, T.; Satz, H. J/ψ Suppression by Quark-Gluon Plasma Formation. *Phys. Lett. B* **1986**, *178*, 416–422. [CrossRef]
3. Rothkopf, A. Heavy Quarkonium in Extreme Conditions. *Phys. Rep.* **2020**, 858, 1–117. [CrossRef]
4. Braun-Munzinger, P.; Stachel, J. (Non)thermal aspects of charmonium production and a new look at J/ψ suppression. *Phys. Lett. B* **2000**, *490*, 196–202. [CrossRef]
5. NA50 Collaboration; Abreu, M.C.; Alessandro, B.; Alexa, C.; Arnaldi, R.; Atayan, M.; Baglin, C.; Baldit, A.; Bedjidian, M.; Beole, S.; et al. Evidence for deconfinement of quarks and gluons from the J/ψ suppression pattern measured in Pb + Pb collisions at the CERN SPS. *Phys. Lett. B* **2000**, *477*, 28–36. [CrossRef]
6. PHENIX Collaboration; Adare, A.; Afanasiev, S.; Aidala, C.; Ajitanand, N.N.; Akiba, Y.; Al-Bataineh, H.; Alexander, J.; Aoki, K.; Aramaki, Y.; et al. J/ψ suppression at forward rapidity in Au+Au collisions at $\sqrt{s_{NN}} = 200$ GeV. *Phys. Rev. C* **2011**, *84*, 054912. [CrossRef]
7. ALICE Collaboration; Adam, J.; Adamova, D.; Aggarwal, M.M.; Aglieri Rinella, G.; Agnello, M.; Agrawal, N.; Ahammed, Z., Ahmad, S.; Ahn, S.U.; et al. J/ψ suppression at forward rapidity in Pb-Pb collisions at $\sqrt{s_{\rm NN}} = 5.02$ TeV. *Phys. Lett. B* **2017**, *766*, 212–224. [CrossRef]
8. Paul, B. ψ(2S) production and nuclear modification factor in nucleus-nucleus collisions with ALICE. In Proceedings of the 41st International Conference on High Energy Physics—ICHEP2022, Bologna, Italy, 6–13 July 2022. [CrossRef]
9. ALICE Collaboration. Letter of intent for ALICE 3: A next-generation heavy-ion experiment at the LHC. *arXiv* **2022**, arXiv:2211.02491.
10. Kharlov, Y. Performance of Calorimetry in ALICE. In Proceedings of the 6th Large Hadron Collider Physics Conference (LHCP 2018), Bologna, Italy, 4–9 June 2018. [CrossRef]
11. Aleksandrov, D.V.; Burachas, S.F.; Ippolitov, M.S.; Lebedev, V.A.; Manko, V.I.; Nikulin, S.A.; Nyanin, A.S.; Sibiriak, I.G.; Tsvetkov, A.A.; Vasiliev, A.A.; et al. A high resolution electromagnetic calorimeter based on lead-tungstate crystals. *Nucl. Instrum. Methods A* **2005**, *550*, 169–184. [CrossRef]
12. ALICE Collaboration; Acharya, S.; Adam, J.; Adamova, D.; Adolfsson Aggarwal, M.M.; Aglieri Rinella, G.; Agnello, M.; Agrawal, N.; Ahammed, Z.; et al. π^0 and η meson production in proton-proton collisions at $\sqrt{s} = 8$ TeV'. *Eur. Phys. J. C* **2018**, *78*, 263. [CrossRef]
13. Skands, P.; Carrazza, S.; Rojo, J. Tuning PYTHIA 8.1: The Monash 2013 Tune. *Eur. Phys. J. C* **2014**, *74*, 3024. [CrossRef]
14. Bierlich, C.; Chakraborty, S.; Desai, N.; Gellersen, L.; Helenius, I.; Ilten, P.; Lönnblad, L.; Mrenna, S.; Prestel, S.; Preuss, C.T.; et al. A comprehensive guide to the physics and usage of PYTHIA 8.3. *SciPost Phys. Codebases* **2022**, *8*.
15. ALICE Collaboration; Acharya, S.; Acosta, F.T.; Adamova, D.; Adhya, S.P.; Adler, A.; Adolfsson, J.; Aggarwal, M.M.; Rinella, G.A.; Agnello, M.; et al. Calibration of the photon spectrometer PHOS of the ALICE experiment. *JINST* **2019**, *14*, P05025. [CrossRef]
16. ATLAS Collaboration; Aad, G.; Abajyan, T.; Abbott, B.; Abdallah, J.; Abdel Khalek, S.; Abdinov, O.; Aben, R.; Abi, B.; Abolins, M.; et al. Measurement of χ_{c1} and χ_{c2} production with $\sqrt{s} = 7$ TeV pp collisions at ATLAS. *JHEP* **2014**, *7*, 154. [CrossRef]